High-Resolution Electron Microscopy Observation of A Solid-Solid Reaction of Tellurium Films with Silver (Commemoration Issue Dedicated to Professor Natsu Uyeda, on the Occasion of His Retirment)

AUTHOR(S):

Shiojiri, Makoto; Isshiki, Toshiyuki; Hirota, Yoshihiro; Okashita, Kazuhiko

CITATION:

Shiojiri, Makoto ...[et al]. High-Resolution Electron Microscopy Observation of A Solid-Solid Reaction of Tellurium Films with Silver (Commemoration Issue Dedicated to Professor Natsu Uyeda, on the Occasion of His Retirment). Bulletin of the Institute for Chemical Research, Kyoto University 1989, 66(5): 517-529

ISSUE DATE:

1989-03-15

URL:

http://hdl.handle.net/2433/77278

Bull. Inst. Chem. Res., Kyoto Univ., Vol. 66, No. 5, 1989

High-Resolution Electron Microscopy Observation of A Solid-Solid Reaction of Tellurium Films with Silver

Makoto SHIOJIRI*, Toshiyuki ISSHIKI**,
Yoshihiro HIROTA*** and Kazuhiko OKASHITA****

Received September 14, 1988

The atomic scale transformation mechanism in Ag-Te films, which grew by a solid-solid reaction of Te films with Ag, has been examined by HRTEM, with the aid of the image simulation and the optical diffraction. By increasing supply of Ag atoms into the Te film, a hexagonal Te lattice transforms to hexagonal $Ag_{2-x}Te_{1+x}$ lattice and then monoclinic $Ag_{2-x}Te$ lattice, with the topotactic relationships of $[100]_{Te}//[100]_{hex}//[010]_{mono}$ and $(001)_{Te}//(001)_{hex}//(100)_{mono}$. The structures of a super-lattice of Te crystal containing interstitial Ag atoms, $Ag_{2-x}Te_{1+x}$ ($x=0.4$) and $Ag_{2-x}Te$ ($x=0.2$) crystals have been determined.

KEY WORDS: Super lattice/ Tellurium/ Topotactic reaction/ Transformation mechanism/ Solid-solid reaction/

I. INTRODUCTION

We have carried out various electron microscopy studies of chalcoginization of metal films in systems such as Ag-S, Cu-Se, Ag-Se, Zn-Se and Cu-Te. In these studies, the topotaxial relationships, the atomic scale growth and transformation mechanism, the morphology and the defect and surface structures in the grown chalcogenides were investigated, as listed in Table 1. A general rule is that the growth and transformation of the chalcogenide crystals proceed by exclusive diffusion of metal ions and electron through the chalcogenide crystals. The structures of crystals such as triclinic and orthorhombic Ag_2Se, $Cu_{4-x}Te$, $Cu_{2-x}Te$ and $Cu_{1-x}Se$ were also determined by means of high-resolution transmission electron microscopy.

In the Ag-Te system, the structures of various crystals were reported as shown in Table 2. Tokody[23] found that the mineral hessite, the low-temperature form of Ag_2Te, has the monoclinic structure. Its detailed structure was described with atomic parameters in $P2_1/c$ cell by Frueh[25]. The orthorhombic structure reported by Rowland and Berry[24] was put aside for a formation of twins. The high-temperature form above 149.5°C has the antifluorite structure similar to those for

* 塩尻 詢 : Department of Physics, Kyoto Institute of Technology, Sakyo-ku, Kyoto 602.
** 一色俊之 : Department of Physics, Kyoto Institute of Technology, Sakyo-ku, Kyoto 602; Present adress: Osaka Prefectural College of Technology, Neyagawa, Osaka.
*** 広田良浩 : Department of Physics, Kyoto Institute of Technology, Sakyo-ku, Kyoto 602; Present adress: Sanyo VLSI Engineering Ltd. Anpachi, Gifu.
**** 岡下和彦 : Department of Physics, Kyoto Institute of Technology, Sakyo-ku, Kyoto 602; Present adress: Sekisui Electronics Laboratory, Tukuba, Ibaragi.

Table 1. Studies of chalcogenization of metal films

System	Metals	Chalcogen	Method	Observation	Ref.
Ag-S	Ag film	S (or H_2S) vapor	CTEM	Topotaxy and tarnishing sites of Ag_2S.	1
			Microbalance	Kinetics.	2
Cu-Se	Cu film	Se film	CTEM	Growth and morphology of CuSe and Cu_2Se.	3
			HRTEM	Defects in Cu_3Se_2.	4, 5
			HRTEM	Growth mechanism of CuSe, Cu_3Se_2 and $Cu_{1.8}Se$.	6, 7
			HRTEM	Transformation mechanism from Se to CuSe; crystal structure of $Cu_{1-x}Se$.	8
Ag-Se	Ag film	Se film	CTEM	Topotaxy of teragonal, orthorhombic and triclinic Ag_2Se.	9
			HRTEM	Crystal structures of triclinic and orthorhombic Ag_2Se; their transformation mechanism.	7, 10
Zn-Se	Zn film	Se film	HRTEM	Polarity and inversion twins in ZnSe.	11, 12, 13
Cu-Te	Cu film	Te film	HRTEM	Transformation mechanism from Te to Cu_xTe, $Cu_{4-x}Te_2$ and $Cu_{2-x}Te$; crystal structures of $Cu_{4-x}Te_2$ ($Cu_{1.6}Te$).	14, 15
				Their grain boundary and surface structure.	16
Ag-Te	Ag film	Te film	HRTEM	Transformation mechanism from Te to $Ag_{5-x}Te_3$ and $Ag_{2-x}Te$; crystal structures of Te(Ag) $Ag_{2-x}Te_{1+x}$ ($Ag_{32}Te_{27}$) and $Ag_{2-x}Te$ ($Ag_{1.8}Te$).	17, The present

Cu_2S and Cu_2Se. Thompson *et al.*[22] systematically examined empressite (discovered in Colorado), stuetzite and a synthetic silver telluride with composition of Ag_5Te_3, on which different structures had been reported[19-21]. They concluded that these tellurides are identical in the structure, having a hexagonal cell of the space group of $P6/mmm$, $a=1.349$ nm and $c=0.848$ nm, and represented by a possible general structural formular of $Ag_{2-x}Te_{1+x}$ ($0.1<x<0.5$).

In the present paper we describe a high-resolution electron microscopy (HRTEM) observation of the solid-solid reaction of Te films with Ag film at room temperature. The transformation mechanism from Te crystal to Ag_2Te crystal is explained at an atomic level, and the structures of a super-lattice of Te crystal containing interstitial Ag atoms, $Ag_{2-x}Te_{1+x}$ ($x=0.4$) and $Ag_{2-x}Te$ ($x=0.2$) crystals are determined by HRTEM. A part of the results has recently been reported[17].

Table 2. The crystal structures of Ag-Te system

Te	Hexagonal	$P3_121$	$a=0.445$, $c=0.591$ nm	Wyckoff[18]
Te(Ag)	Superstructure of Te		$a=1.335$, $c=0.591$ nm	The present
Stuetzite or empressite				
AgTe	Orthorhombic	Pmnm or Pmn	$a=0.890$, $b=2.007$, $c=0.462$ nm	Honea[19]
$Ag_{12}Te_7$	Hexagonal		$a=1.3457$, $c=0.84685$	Koern[20]
$Ag_{5-x}Te_3$	Hexagonal	P6/mmm	$a=1.349$, $c=0.848$ nm	Berry et al.[21]
			$a=1.338$, $c=0.845$ nm	Honea[19]
$Ag_{2-x}Te_{1+x}$ $(0.1<x<0.5)$		P6/mmm	$a=1.349$, $c=0.848$ nm	Thompson et al.[22]
$Ag_{32}Te_{27}$		P6/mmm	$a=1.34$, $c=0.84$ nm	The present
$Ag_{2-x}Te$ $(x=0.2)$	Monoclinic	$P2_1/c$	$a=0.74$, $b=0.448$ $c=0.84$ nm, $\beta=123°20'$	The present
Hessite				
Ag_2Te	Monoclinic	P2 or P2/m	$a=0.657$, $b=0.614$, $c=0.610$ nm, $\beta=61°15'$	Tokody[23]
	Orthorhombic	Immm	$a=1.628$, $b=2.668$, $c=0.755$ nm	Rowland and Berry[24]
	Monoclinic	$P2_1/c$	$a=0.809$, $b=0.448$, $c=0.896$ nm, $\beta=123°20'$	Frueh[25]
Ag_2Te (high-temperature phase)	Cubic	antifluorite	$a=0.6572$ nm	Ralfs[26]

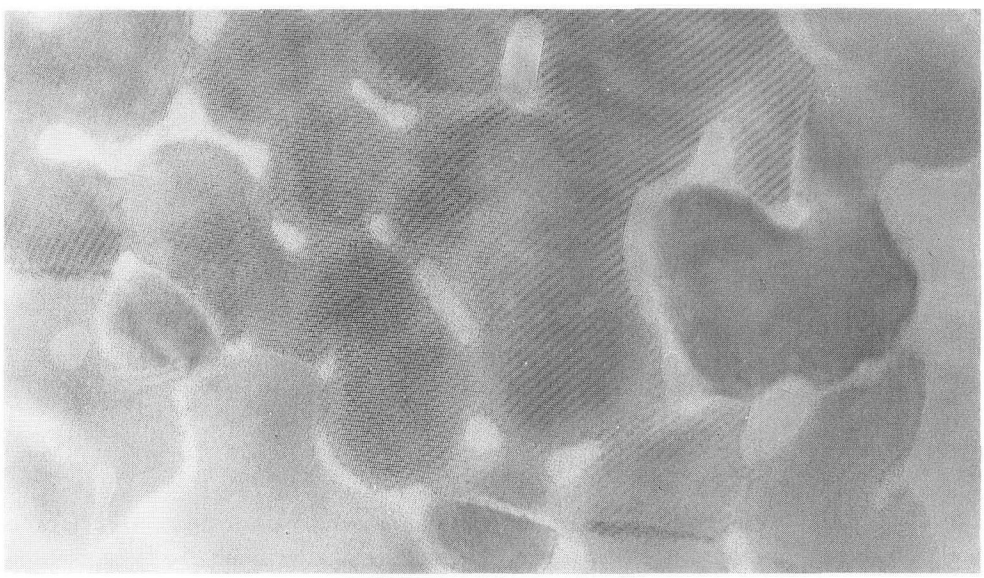

(a)

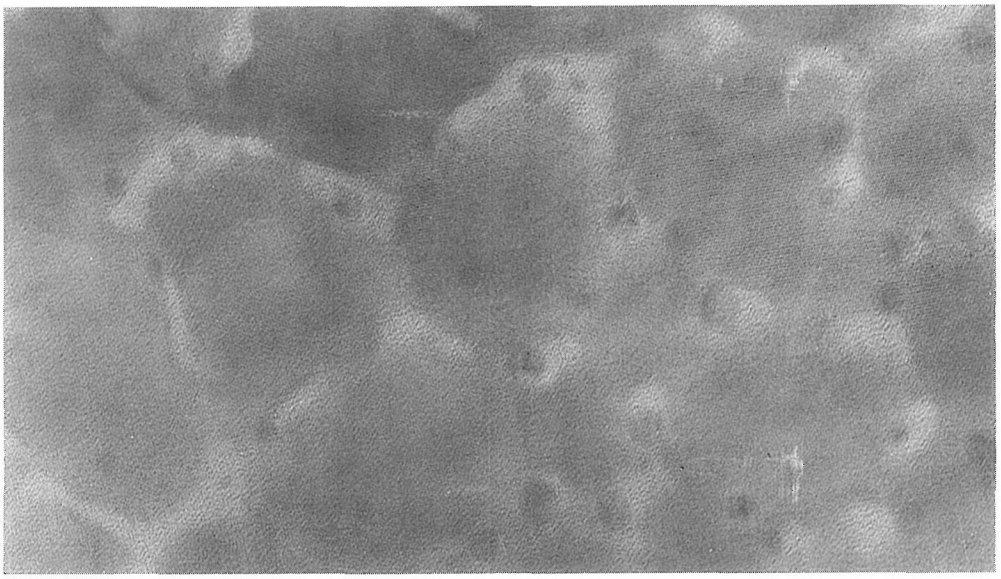

(b)

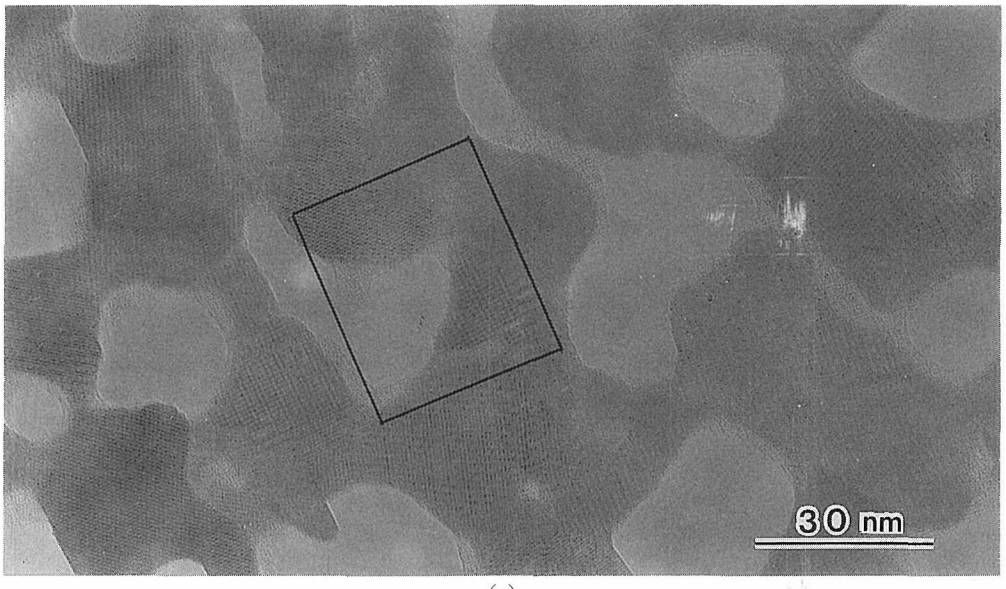

(c)

Fig. 1. (a): A vacuum-deposited Te film 20 nm thick. (b): A Te film immediately after Ag was deposited on it. (c): The Te film 2 hr after the preparation. The area indicated by the rectangle corresponds to the area in Fig. 2.

II. EXPERIMENTAL

A Te film 20 nm thick was prepared by vacuum-deposition onto a surface of a KCl crystal at room temperature, and immediately after then Ag was vacuum-deposited on the Te film. The mean thickness of Ag was 1 nm. The film was

wet-stripped from the substrates and mounted on a holey film for HRTEM. Ag-Te crystals produced in the film at room temperature were observed with a JEM-200CX electron microscope (Cs=1.2 mm). Image simulation was made on a computer by multi-slice method[27,28] with an ACOS-850 at the Data Processing Center,

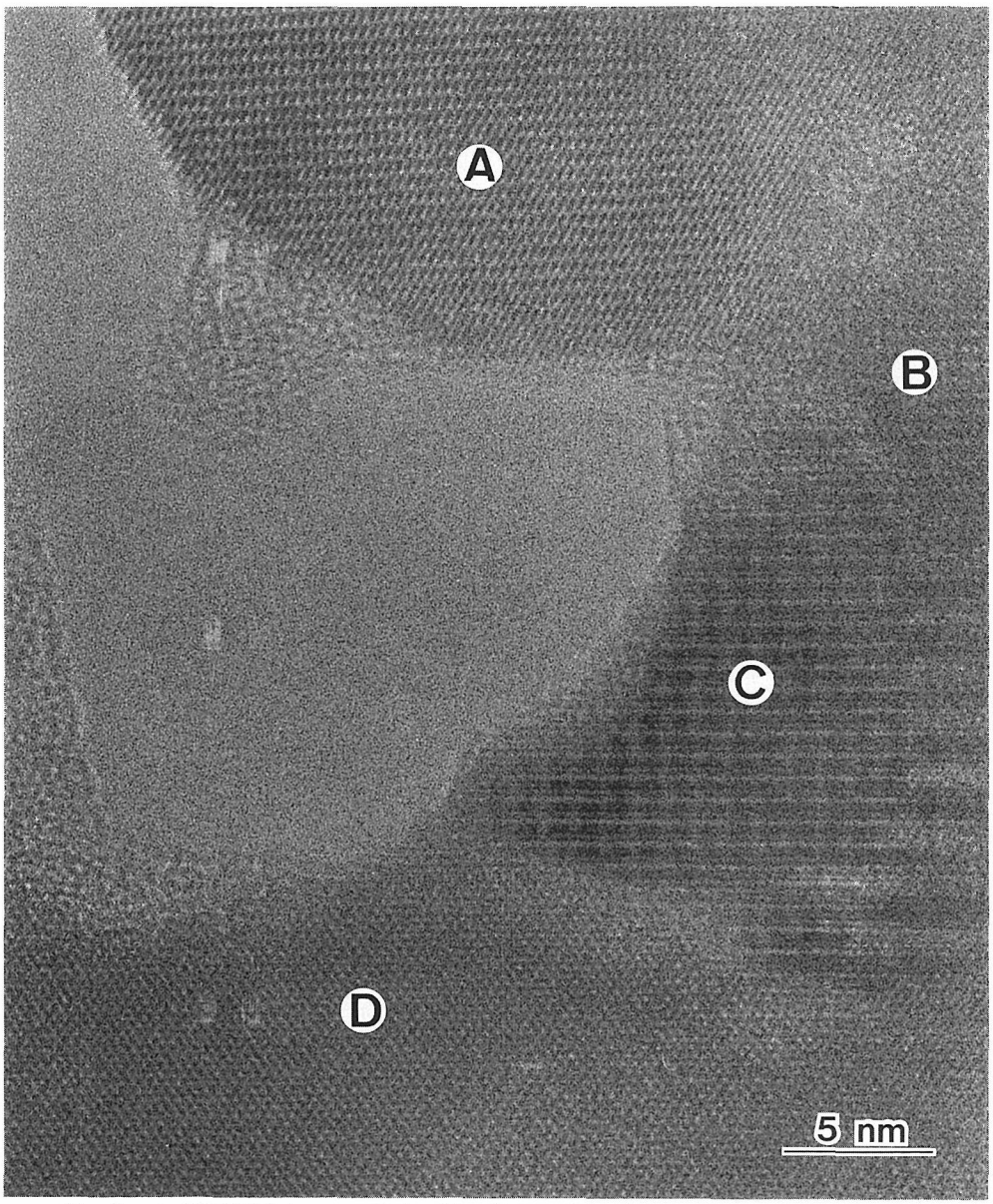

Fig. 2. A HRTEM image of the film 2 hr after the specimen preparation. A hexagonal Te [100]-crystal (at A), a [100]-Te(Ag) crystal having a superlattice structure (at B), a hexagonal [100]-$Ag_{2-x}Te_{1+x}$ crystal (at C) and a *monoclinic* [010]-$Ag_{2-x}Te$ *crystal* (at D) are seen.

Kyoto Institute of Technology. The calculation was carried out under the following conditions: $E=200\,\mathrm{kV}$; $Cs=1.2\,\mathrm{mm}$; beam divergence 10^{-4} (semi-angle). For the half-width of the defocus fluctuation of the microscope (mainly caused by energy spread), which acts on the objective lens envelope function, 10 nm was assumed to be a reasonable value. Values of underfocus Δf were assigned using the manufacture's figure for the steps of the objective lens current knob, and absolute values were determined by comparison with simulated images. The optical diffraction of the images was carried out to measure the lattice spacings of the crystals locally produced.

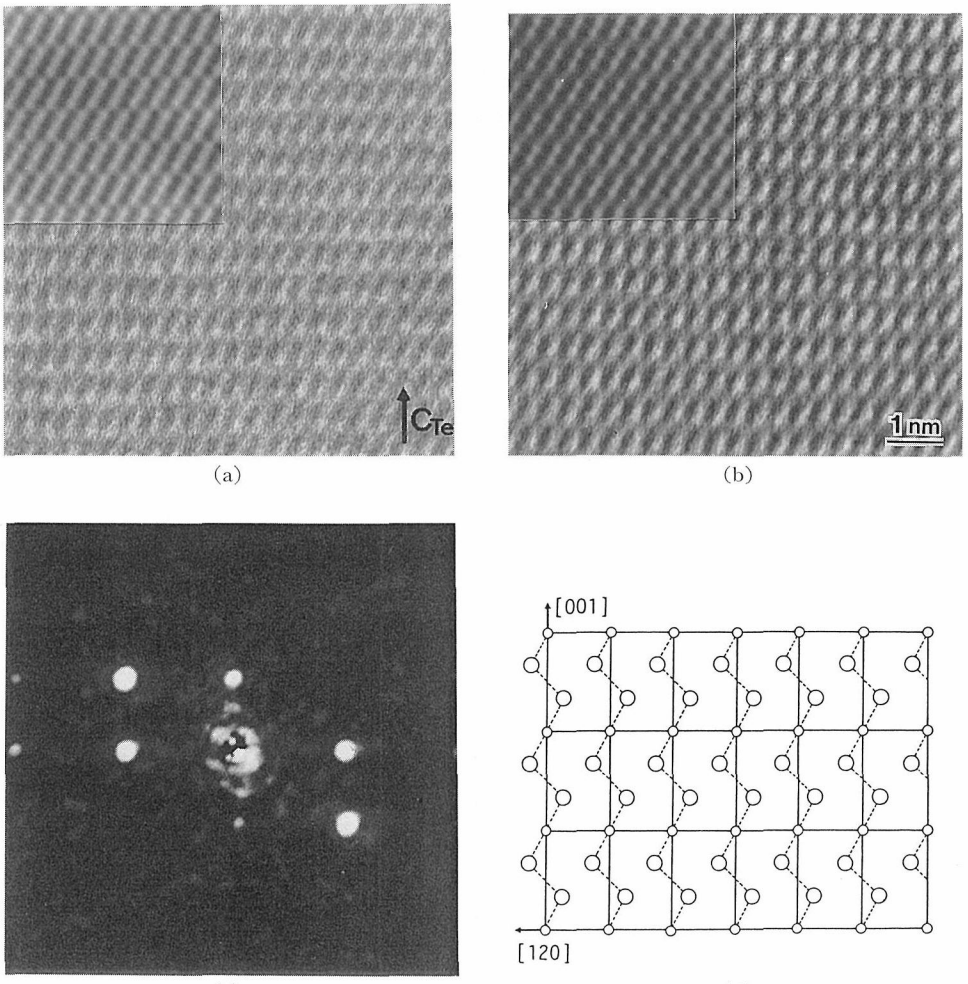

(a) (b) (c) (d)

Fig. 3. (a) and (b): Observed and calculated images of the [100]-Te crystal 20 nm thick at A in Fig. 2, at underfocuses of $\Delta f=15$ and 60 nm. (c): An optical diffractogram of the observed image. (d): The projection of Te crystal along the [100]-axis.

III. RESULTS AND DISCUSSION

Figure 1 (a) shows a Te film 20 nm thick, vecuum-deposited on a KCl surface at room temperature. The Te film, immediately after Ag was deposited on it, is shown in Fig. 2 (b). The Ag particles are seen as black spots a few nanometers in size. Fig. 1 (c) shows the Te film 2 hr after the preparation. Various silver telluride crystals in different reaction stages, were formed by the migration of Ag atoms into the Te film. Figure 2 shows an enlarged image of the area enclosed by a rectangle in Fig. 1 (c). A hexagonal [100]-Te crystal, a [100]-Te(Ag) crystal having a super-lattice structure, a hexagonal [100]-$Ag_{2-x}Te_{1+x}$ crystal and a

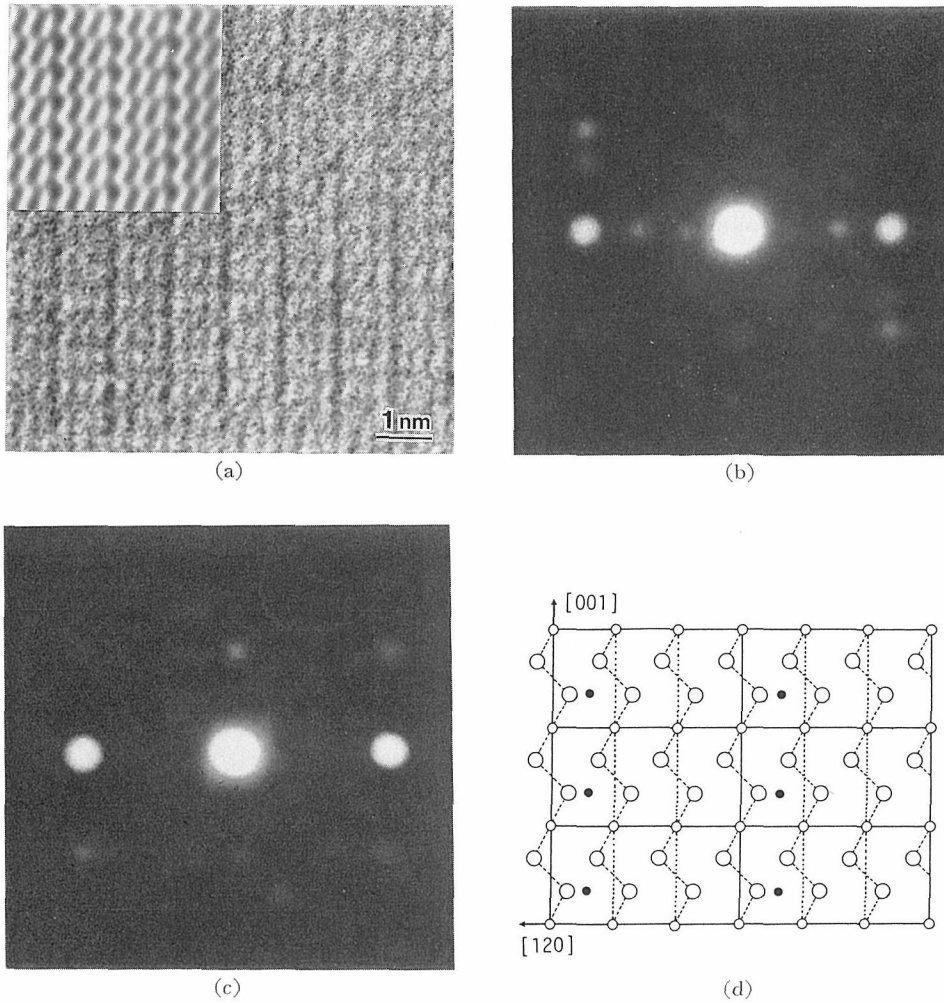

Fig. 4. (a): An enlarged observed image of the [100]-Te(Ag) crystal at B in Fig. 2. Inset is the calculated image for the Te(Ag) crystal shown in Table 3, at Δf=55 nm. (b): An optical diffractogram of the observed image. (c): The reference diffractogram of the image of Te crystal. (d): The atom projection of the Te(Ag) crystal.

monoclinic [010]-$Ag_{2-x}Te$ crystal, as mentioned below, appear at A, B, C, and D, respectively.

Figs. 3 (a) and (b) are observed and calculated images of the [100]-Te crystal at A in Fig. 2, at underfocuses of $\Delta f=15$ nm and 60 nm. The calculations were carried out for the hexagonal Te crystal 20 nm thick (see Table 3). The atom projection of the Te crystal along the [100]-axis is indicated in Fig. 3 (d). The Te crystal is an aggregate of endless zig-zag chains, which are arranged spirally about the c-axis of the unit cell. The zig-zag chains of the Te atoms can distinctly be seen in HRTEM images. Fig. 3 (b) shows an optical diffractogram of the observed image. We used it for the calibration of the spacings in the diffractograms from the lattice fringes in the other crystals.

Figure 4 (a) shows an enlarged image of the crystal at B in Fig. 2. The optical diffractogram of the observed images is shown in Fig. 4 (b). Fig. 4 (c) is the reference diffractogram of the image of the Te crystal appearing in the same photo film. It is deduced that the crystal has the same spacings as those of Te crystal but its lattice fringes are modulated in a period of $3a_{Te}$, where a_{Te} is the lattice constant of the Te crystal. We then assumed that Ag atoms are periodically distributed among the three Te chains, forming a superstructure. A similar

Table 3. Crystal data used for image calculations

Crystal	Coordinates	Image
Te* Hexagonal $P3_121$ $a_{Te}=0.445$, $c_{Te}=0.591$ nm	Te(3): u, 0,0 ; $\bar{u}$, $\bar{u}$, 1/3; 0, u, 2/3 u=0.269	Fig. 3
Te(Ag)** Superstructure of Te $a=a_{Te}$, $b=3a_{Te}$, $c=c_{Te}$	Te(9): 0, $u/3$, 2/3; u, 0, 0; $\bar{u}$, $(1+\bar{u})/3$, 1/3; 0, $(1+u)/3$, 2/3; u, 1/3, 0; u, $(2+u)/3$, 1/3; 0, $(2+u)/3$, 2/3; u, 2/3, 0; $\bar{u}$, $(3+\bar{u})/3$, 1/3 Ag(1): v, $2v/3$, 1/3 $u=0.259$, $v=0.562$	Fig. 4
$Ag_{2-x}Te_{1+x}$ ($x=0.4$)** ($=Ag_{32}Te_{27}$) Hexagonal P6/mmm $a=1.34$, $c=0.84$ nm	Te(27): 0, 0, 0; $\pm u$, 0, 0; 0, $\pm u$, 0; 0, 0, $\pm u$; $\pm u$, $\pm u$, 0; $\pm u$, $\mp u$, 0; $\pm u$, 0, $\pm u$; $\pm u$, 0, $\mp u$; 0, $\pm u$, $\pm u$; 0, $\pm u$, $\mp u$; $\pm u$, $\pm u$, $\pm u$; $\pm u$, $\pm u$, $\mp u$; $\pm u$, $\mp u$, $\pm u$; $\pm u$, $\mp u$, $\mp u$ $u=1/3$ Ag(32): $\pm v$, $\mp v$, 0; v, v, 0; $\pm v$, 1/2, 0; 1/2, $\pm v$, 0; $\pm w$, $\mp w$, $\pm v$; w, $\bar{w}$, $\bar{v}$; $\pm 2w$, $\pm w$, $\mp v$; $2\bar{w}$, $\bar{w}$, $\bar{v}$; $\pm w$, $\pm 2w$, $\pm v$; w, $2w$, $\bar{v}$; $\pm 2w$, $\mp 2w$, $\mp v$; $\pm 2w$, $\pm 4w$, v; $2\bar{w}$, $4\bar{w}$, v; $\pm 4w$, $2w$, $\pm v$; $\pm 4w$, $\pm 2w$, $\pm v$; $\pm w$, $\pm 4w$, $\pm v$; w, $4\bar{w}$, $\bar{v}$; $4w$, $\bar{w}$, $\pm v$; $\pm 4w$, w, $\bar{v}$ $v=0.167$, $w=0.111$	Fig. 5
$Ag_{2-x}Te$ ($x=0.2$)** Monoclinic $P2_1/c$ $a=0.74$, $b=0.45$ $c=0.84$ nm, $\beta=123°20'$	Te(1): 0.272, 0.159, 0.243 Ag(<2): 0.25, 0.659, 0.493; 0.5, 0.659, 0.410; 0.5, 0.659, 0.576 Cu was used for as an average atom equivalent to having some Ag and some vacancy present.	Fig. 6

* Ref. 18).

** Structures newly determined in the present investigation.

structure has been found in the early stage of the reaction of Te films with Cu[15]. From the image simulation, we propose a model structure, whose atom projection is indicated in Fig. 4 (d). Ag atoms occupy every three interstices of the Te chains. The atomic configuration is shown in Table 3. A calculated image, at Δf=55 nm, for this crystal 20 nm thick is inset in Fig. 4 (a) and this accounts for the observed image.

The area C in Fig. 2 can be identified to be the hexagonal $Ag_{2-x}Te_{1+x}$ crystal reported by Berry and Thompson[21] (ASTM card 18-1187), although the lattice constants are a little different. Figs. 5 (a) and (b) are observed images of the [100]-$Ag_{2-x}Te_{1+x}$ at Δf=40 and 85 nm, respectively. Fig. 5 (c) is an optical dif-

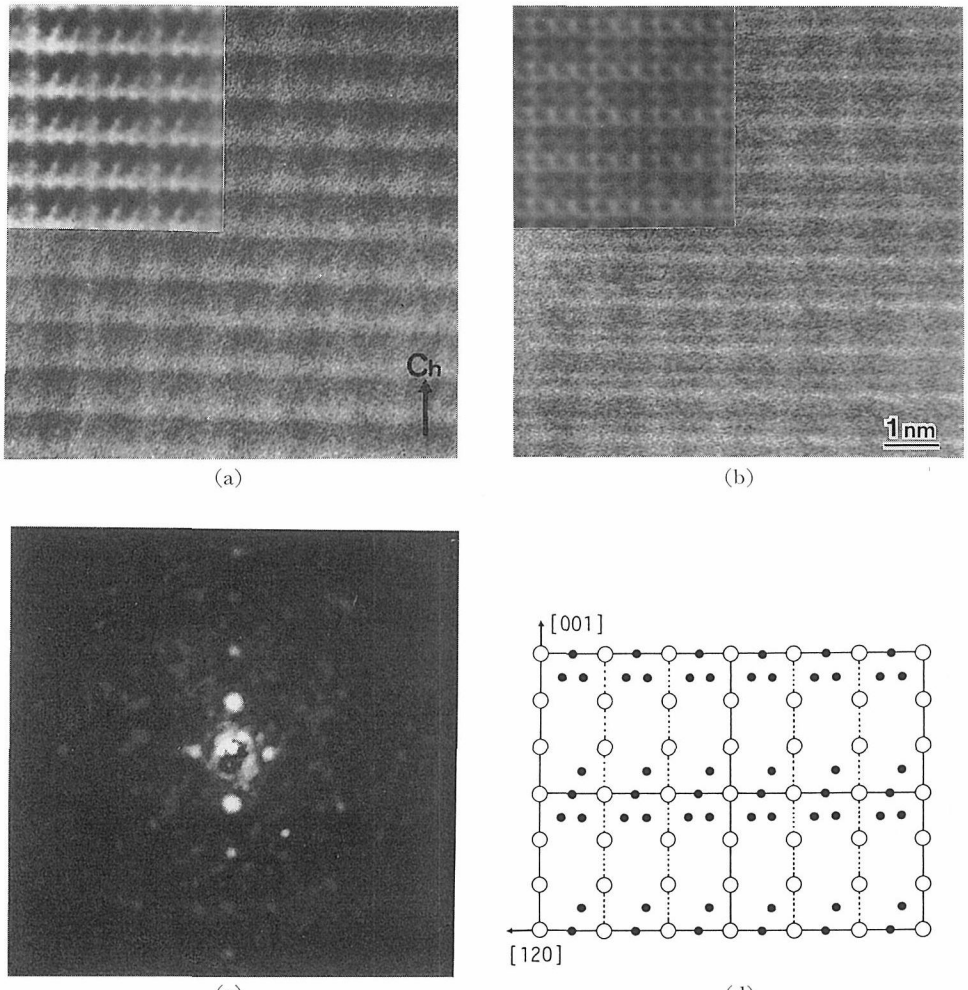

Fig. 5. (a) and (b): Observed images and calculated images (insets) of the [100]$Ag_{2-x}Te_{1+x}$ crystal at C in Fig. 2, at Δf=40 nm and 85 nm. (c): An optical diffractogram of the observed image. (d): The projection of the $Ag_{2-x}Te_{1+x}$ ($Ag_{32}Te_{27}$) crystal along the [100]-axis.

fractogram of the observed image. There is no report on the atomic configuration in the hexagonal unit cell. We obtained calculated images which can account for the observed images satisfactorily. The calculated images are inset in Figs. 5 (a) and (b). The structure data for the calculation are shown in Table 3 and the atom projection along the [100]-axis is indicated in Fig. 5 (d). In the unit cell, 32 Ag atoms and 27 Te atoms are placed so that the composition is $Ag_{1.6}Te_{1.4}$ ($x=0.4$ in $Ag_{2-x}Te_{1+x}$).

The area D in Fig. 2 is a crystal having a monoclinic lattice. The image could not be regarded as the image from the monoclinic Ag_2Te crystal reported by Frueh[25]. The observed images at $\Delta f=40$ and 85 nm are shown in Figs. 6 (a)

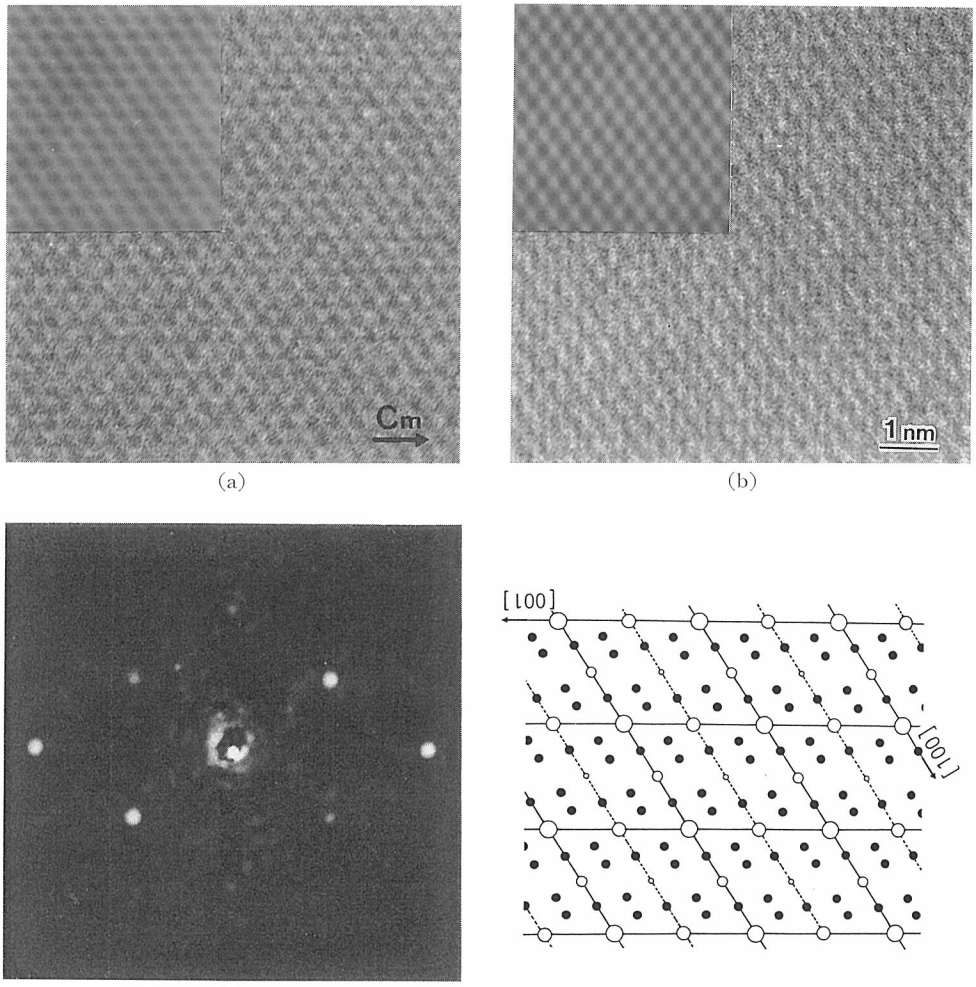

Fig. 6. (a) and (b): Observed images and calculated images (insets) of the [100]-$Ag_{2-x}Te$ crystal at D in Fig. 2, at $\Delta f=40$ nm and 85 nm. (c): An optical diffractogram of the observed image. (d): the projection of the $Ag_{2-x}Te$ ($Ag_{1.8}Te$) crystal along the [010]-axis.

and (b), and an optical diffractogram in Fig. 6 (c). We determined the lattice constants of the present crystal to be $a=0.74$, $b=0.448$, $c=0.84$ nm and $\beta=123°20'$. Since its unit cell is smaller than that of the stoichiometric Ag_2Te crystal, it might contain some Ag vacant sites. The calculated images inset in Figs. 6 (a) and (b) are taken for the best matched ones with the observed images. The calculations were carried out for an $Ag_{1.8}Te$ crystal, whose structure data is shown in Table 3 and the atom projection along the [010]-axis is shown in Fig. 6 (d). Te atoms occupy (4*e*) sites (having different parameters from those of the Ag_2Te crystal[25]) in the $P2_1/c$ cell and Ag atoms randomly occupy three different (4*e*) sites with a probability less than 2/3. On the calculation, Cu was used for as an average atom equivalent to having some Ag and some vacancy present.

The observed Te(Ag), $Ag_{2-x}Te_{1+x}$, and $Ag_{2-x}Te$ crystals were produced by a solid-solid reaction of the Te film with Ag migrating to it, similar to the other

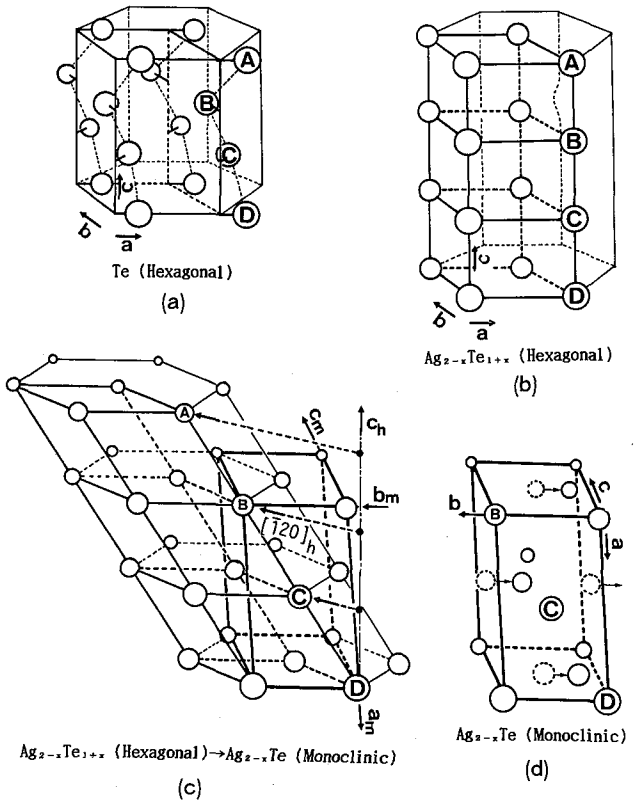

Fig. 7. (a): The lattice of the hexagonal Te crystal. (b): The Te sub-lattice of the hexagonal $Ag_{2-x}Te_{1+x}$ crystal. (c): The deformation of the Te sub-lattice on the transformation from the $Ag_{2-x}Te_{1+x}$ to the $Ag_{2-x}Te$ crystal. (d): The Te sub-lattice of the monoclinic $Ag_{2-x}Te$ crystal. A, B, C and D represent the change of the zig-zag chain of Te atoms in the Te crystal through the transformation.

chalcogenizations of metals[3–16]. The produced crystals were transformed with the following topotaxial relationship:

$$[100]_{Te}//[100]_{Ag_{2-x}Te_{1+x}}//[010]_{Ag_{2-x}Te}$$
$$(001)_{Te}//(001)_{Ag_{2-x}Te_{1+x}}//(100)_{Ag_{2-x}Te}.$$

The lattice of the Te crystal and the Te sub-lattices of the hexagonal $Ag_{2-x}Te_{1+x}$ and the monoclinic $Ag_{2-x}Te$ crystals are shown in Figs. 7 (a), (b), and (d), respectively. In conclusion, the reaction of Te film with Ag is summarized as follows. In the initial stage of the reaction, Ag atoms are introduced in the tunnels among three Te chains and Ag walls are built parallel to the $(010)_{Te}$-plane. As the Ag walls are ordered, the crystal has a superlattice structure with $a=3a_{Te}$, as seen at B in Fig. 2. By further supplying of Ag atoms, the Te chains are completely stretched and the $Ag_{2-x}Te_{1+x}$ crystal forms, as shown in Fig. 7 (b). The Te sublattice still has the hexagonal cell coming from the super-lattice with $a=3a_{Te}$. The (001) layers with Ag atoms and without Ag atoms are periodically stacked among the Te sub-lattice. As the layers are filled with increasing supply of Ag atoms, the hexagonal $Ag_{2-x}Te_{1+x}$ crystal may change to the $Ag_{2-x}Te$ crystal. The transformation can be explained to take place by successive slipping of the Te atoms on the (001) planes toward $[120]_h$ and their relative displacement, as schematically shown in Fig. 7 (b). The Ag positions in the present $Ag_{2-x}Te$ crystal are different from those in the stoichiometric Ag_2Te which are 0.018, 0.152, 0.371 and 0.332, 0.837, 0.995[25]. The Te sub-lattice and the Ag atom sites change by the further supply of Ag atoms, forming the stoichiometric Ag_2Te.

We would like to express our thanks to Mr. S. Sekimoto who developed the computer program used for the image simulation.

RFERENCES

(1) M. Shiojiri, S. Maeda and Y. Murata, *Jpn. J. Appl. Phys.*, **8**, 24 (1969).
(2) M. Shiojiri, Y. Hasegawa, Y. Murata and S. Matsumura, *Jpn. J. Appl. Phys.*, **8**, 783 (1969).
(3) H. Morikawa, *Jpn. J. Appl. Phys.*, **9**, 607 (1970).
(4) H. Morikawa, M. Shiojiri and E. Suito, *J. Appl. Phys.*, **42**, 2143 (1971).
(5) H. Morikawa, *Jpn. J. Appl. Phys.*, **11**, 431 (1972).
(6) M. Shiojiri, C. Kaito, Y. Saito, K. Teranishi and S. Sekimoto, *J. Crystal Growth*, **52**, 883 (1981).
(7) M. Shiojiri, C. Kaito, S. Sekimoto, K. Teranishi and N. Nakamura, in: Electron Microscopy 1982, Proc. 10th Intern. Congr. on Electron Microscopy, Hamburg, 1982, Vol. 1 (Deut. Ges. Elektronemikroskopie, Frankfurt, 1982) p. 207.
(8) M. Shiojiri, Y. Hirota, K. Okashita and S. Sekimoto, in: Recent Development of Electron Microscopy 1987, Proc. 4th Chinese-Japanese Electron Microscopy Seminar, Kunming, 1987 (Business Center Academic Soc. Jpn., Tokyo, 1988) p. 33.
(9) Y. Saito, M. Sato and M. Shiojiri, *Thin Solid Films*, **79**, 257 (1981).
(10) C. Kaito, N. Nakamura, K. Teranishi, S. Sekimoto and M. Shiojiri, *Phys. Stat. Sol.* (*a*), **71**, 109 (1982).
(11) M. Shiojiri, C. Kaito, S. Sekimoto and N. Nakamura, *Phil. Mag. A*, **46**, 495 (1982).
(12) C. Kaito, N. Nakamura, S. Sekimoto and M. Shiojiri, in: Electron Microssopy 1982, Proc. 10th Intern. Congr. on Electron Microscopy, Hamburg, 1982, Vol. 1 (Deut. Ges. Elektronenmikroskopie, Frankfurt, 1982) p. 339.
(13) M. Shiojiri, in: Proc. 7th Intern. Summer School Defects in Crystals, Szczyrk (Poland), 1985 (World Sci. Pub., Singapore, 1987) p. 291.

(14) T. Isshiki, K. Okashita, Y. Hirota, T. Maeda, S. Sekimoto and M. Shiojiri, in: Electron Microscopy 1986, Proc. 11th Intern. Cogr. on Electron Microscopy, Kyoto, 1986, Vol. 1 (Jpn. Soc. Electron Micros., Tokyo, 1986) p. 865.
(15) M. Shiojiri, T. Isshiki, K. Okashita, Y. Hirota, T. Maeda and S. Sekimoto, *J. Crystal Growth*, **83**, 421 (1987).
(16) M. Shiojiri, T. Isshiki, K. Okashita, Y. Hirota, T. Maeda and S. Sekimoto, *Ultramicroscopy*, **23**, 355 (1987).
(17) M. Shiojiri, K. Okashita, Y. Hirota, S. Sekimoto and H. Obatake, in: Electron Microscopy 1988, Proc. 4th Asia-Pacific Confer. and Workshop on Electron Microscopy, Bangkok, 1988 (Electron Micros. Soc. Thailand, Bangkok, 1988) p. 155.
(18) R.G. Wyckoff, Crystal Structures, 2nd ed. (Interscience, New York, 1965) p. 36.
(19) R.M. Honea, *Amer. Mineral.*, **49**, 325 (1964).
(20) V. Koern, *Naturwiss.*, **27**, 432 (1939).
(21) L.G. Berry and R.M. Thompson, *Geol. Soc. Amer. Mem.*, **85**, (1962).
(22) R.M. Thompson, M.A. Peacok, J.F. Rowland and L.G. Berry, *Amer. Mineral.*, **36**, 458 (1951).
(23) L. Tokody, *Z. Kristallogr.*, **82**, 154 (1932); **89**, 416 (1934).
(24) J.F. Rowland and L.G. Berry, *Amer. Mineral.*, **36**, 471 (1951).
(25) A.J. Frueh, *Z. Kristallogr.*, **112**, 44 (1959).
(26) P. Ralfs, *Z. Phys. Chem. B*, **31**, 157 (1936).
(27) J.M. Cowley and A.F. Moodie, *Acta Crystallogr.*, **10**, 619 (1957).
(28) P. Goodman and A.F. Moodie, *Acta Crystallogr.*, **A30**, 280 (1974).